RSC Pharmaceutics

ROYAL SOCIETY OF CHEMISTRY

PAPER

View Article Online
View Journal | View Issue

Cite this: *RSC Pharm.*, 2024, **1**, 498

Development of a naproxen and gaultheria oil based topical nanoemulsion for the amelioration of osteoarthritis†

Abdul Nafey Faheem, ‡ Ahsan Ali, Athar Shamim, ‡ Sradhanjali Mohapatra, Ayesha Siddiqui, Zeenat Iqbal * and Mohd. Aamir Mirza*

Osteoarthritis (OA) is a chronic degenerative condition characterized by the wearing down of the articulating surfaces of the tibia–femoral joint. It involves the breakdown of cartilage, leading to a reduction in joint space, primarily affecting the medial aspect of the joint. Treatment options for OA include oral and topical medications, as well as chemical and surgical interventions. Among potential treatments, naproxen (NAP) and gaultheria oil (GO) have shown promising anti-inflammatory effects. However, NAP's distribution is hindered by its limited solubility and poor penetration. Additionally, there is no marketed product or published report of any combination product of GO with any synthetic drug. Hence a novel nanoemulsion (NE) based gel has been developed. For NE development, Tween 80 and PEG 400 were selected as the surfactant and co-surfactant, respectively. The particle size, polydispersity index (PDI) and zeta potential were found to be 209.2 nm, 0.2119, and −24.7 mV respectively. *In vitro* cumulative drug release in the initial 24 h was 95.64 ± 0.75% for NE and 87.44 ± 0.84% for NEG. Similarly, *in vitro* drug permeation after 24 h was 17.447 μg cm^{-2} and 9.3287 μg cm^{-2}, respectively. The rheological behavior, skin irritation, and stability of the NEG were also evaluated.

Received 25th February 2024,
Accepted 22nd April 2024

DOI: 10.1039/d4pm00059e

rsc.li/RSCPharma

1. Introduction

Osteoarthritis (OA) is a prevalent musculoskeletal disorder that affects the joints and is characterized by a common musculoskeletal condition that affects joints by cartilage degradation and joint inflammation, which can cause pain, stiffness, and decreased mobility.[1] The etymology of "arthritis" is derived from the Greek word "arthron" for joint and the Latin word "itis" for inflammation.[1] While traditionally perceived as a localized cartilage disease, recent insights have illuminated OA as a multifaceted joint disorder, involving synovial fluid, articular cartilage, and surrounding tissues.[2,3]

Among the various manifestations of OA, knee osteoarthritis (KOA) has emerged as a prominent public health concern, causing significant disability and societal burden.[4] Cartilage degeneration and inflammation within knee joints lead to pain, stiffness, and reduced mobility, impairing patients' functional abilities.[1] In India, KOA has garnered special attention due to its high prevalence, straining healthcare resources and complicating disability management.[5,6]

As the global population ages and risk factors evolve, OA's prevalence is surging. The synergy of aging, increased obesity rates, sedentary lifestyles, and other factors contribute to the escalation of the OA epidemic.[7] This evolving epidemiological landscape underscores the urgency of understanding OA's origins, impact, and public health implications.

While treatment strategies for OA encompass medications, physical therapy, lifestyle modifications, and surgical interventions, they are not without challenges. The efficacy of pharmacological treatments like non-steroidal anti-inflammatory drugs (NSAIDs) and analgesics can be limited by potential side effects, including various health risks.[8] Physical therapy and exercise, while being effective, require patient adherence and may not completely halt disease progression.[9] Surgical options, such as joint replacement, provide relief but entail substantial costs, invasive procedures, and post-operative complications[9] Topical delivery has emerged as an alternative to conventional drug delivery methods for substances like analgesics, hormones, scopolamine, and nicotine.[10,11] This approach offers the advantage of circumventing first-pass hepatic metabolism, thereby enhancing bioavailability.[12,13]

Department of Pharmaceutics, School of Pharmaceutical Education and Research, Jamia Hamdard, New Delhi, 110062, India. E-mail: aamir_pharma@yahoo.com, zeenatiqbal@jamiahamdard.ac.in

†Electronic supplementary information (ESI) available: Table S1: solubility of NAP in different surfactants and co-surfactants, and HLB values of selected surfactants; Table S2: summary of regression analysis findings for responses R1, R2 and R3 for quadratic equation fitting and Fig. S1: observation of stress stability studies of different formulations. See DOI: https://doi.org/10.1039/d4pm00059e

‡Both the authors have contributed equally and hence should be considered as the first authors.

Various techniques have been used to improve drug permeation through topical delivery. These methods include iontophoresis, microneedle technology, and electroporation. However, these techniques often prove to be economically unfeasible.[12,13] A myriad of challenges underscore the necessity for developing safe, effective, and economical topical formulations. Nano-emulsions (NE) offer remarkable potential in enhancing the topical delivery of BCS class II drugs due to their exceptional solubilization capabilities. NE with higher oil content exhibit enhanced penetration of lipophilic drugs.[14] Nano-emulsion gel (NEG) systems provide a range of advantages as topical delivery platforms, negating the need for additional penetration enhancers. The NE component enhances percutaneous permeation and demonstrates the combined properties of NE and hydrogels. NEG exhibits faster drug release rates compared to creams and ointments, while maintaining a consistent and homogeneous behaviour.[14]

NAP, an effective non-steroidal anti-inflammatory drug (NSAID), is used in the treatment of various musculoskeletal disorders like arthritis, traumatic contusions, and dysmenorrhea.[15] Its chemical formula is 6-methoxy-α-methyl-2-naphthalene acetic acid, and the recommended clinical oral dose ranges from 0.75 to 2.25 g day^{-1}. However, NAP has limited water solubility (around 15.9 mg L^{-1} at 25 °C, log P = 3.18) and a relatively extended elimination half-life (12–14 h), which lead to reduced efficacy.[16] To enhance the therapeutic effectiveness, it is crucial to address these issues by reducing its size and utilizing surfactants to improve its solubility. GO is rich in methyl salicylate, a prominent constituent that helps to exert anti-inflammatory activity. This compound finds application in different therapeutic contexts, including the treatment of rheumatic arthritis, sciatica, and neuralgia. It is a common ingredient in proprietary balms, liniments, and ointments.[17] GO, when applied topically, can permeate through the skin and underlying tissues. Its mechanism involves the reversible inhibition of the cyclooxygenase enzyme at the local level. This action impedes the peripheral production of inflammatory mediators, including prostaglandin and thromboxane A2, thus presenting a potential synergistic effect.[18]

The present research aims to assess the potential of a NE containing NAP and GO as an oil phase for OA treatment. This innovative approach harnesses the benefits of nanotechnology. Furthermore, the synergistic effect arising from the combined action of these two components adds an intriguing dimension to the exploration of this NE-based approach.

2. Materials and methods

2.1. Materials

Naproxen was obtained as a complimentary sample from Sun Pharmaceutical Industries Limited, Gurgaon (India), while Gaultheria oil was procured from SM Classy Sahibabad Industrial Area Site 4, Sahibabad, Ghaziabad. Tween 80 and PEG 400 were procured from Merck, Mumbai (India). A cellulose dialysis bag with a molecular weight cutoff of 12 KD was sourced from Sigma Aldrich, Bangalore (India). Additionally, a nylon membrane filter (0.45 μm) was purchased from Sigma Aldrich Chemicals Private Limited, Bangalore, India. Throughout the study, Milli Q water was consistently used. All chemicals employed in the experiment were of analytical grade.

2.2. Methods

On the basis of the solubility of NAP in different essential oils, surfactants and co-surfactants of the nanoemulsion formulation were selected. With the help of a pseudo-ternary phase diagram the NE region was identified, furthermore NE was optimized using design of experiments (DOE). Finally, the developed NE was incorporated into a Carbopol gel for topical administration. The characterization of the drug-loaded NE and NEG was performed using various techniques, including transmission electron microscopy (TEM), zeta potential analysis, pH measurement, rheological behaviour assessment, *in vitro* drug release studies, *ex vivo* permeation studies on Wistar rat skin, confocal laser scanning microscopy and stability studies.

2.3. Screening of NE ingredients

The solubility of NAP was assessed in different oils (apricot oil, gaultheria oil, lemongrass oil, clove oil, and kalonji oil). Excess NAP was added to 2 ml of selected oil in Eppendorf tubes and mixed using a vortex mixer. The mixture was then shaken on an isothermal shaker at 25 ± 1 °C for 72 hours. Afterward, centrifugation at 3000 rpm for 15 minutes was performed, and the final supernatant was filtered through a syringe filter (0.22 μm). The drug content was analysed at 232 nm using a UV spectrophotometer.[19,20]

To identify the most effective surfactant for the oil system, a series of emulsions were prepared using different surfactants. The oil which exhibited the highest drug solubility was selected. The evaluation of surfactant emulsification capacity involved gradually adding the oil phase (5 μl) to a 20% aqueous surfactant solution (1 ml) drop by drop. A vortex mixer was used to mix after each addition until the two phases remained homogeneous. This process continued until the mixture turned turbid, at which point it was left undisturbed for 24 hours. Visual inspection was then carried out to check for any signs of turbidity or phase separation.[21]

The inclusion of co-surfactants, alongside the chosen surfactant, was found to be beneficial. This combination reduced interfacial tension and enhanced interface fluidity, facilitating the formation of NE through a low-energy emulsification approach. Furthermore, it enabled the formulation of NE with minimal surfactant concentration.

2.4. Development of pseudo-ternary phase diagrams

A phase behaviour study of the selected ingredients including the oil, aqueous phase, and surfactant mixture, was conducted through the construction of a phase diagram.[22] This phase diagram takes the form of a ternary plot and is generated by subjecting the mixture of oil and the surfactant–cosurfactant

blend (S_{mix}) to aqueous titration. During this process, water is added drop by drop, with intermittent stirring, and the resulting phase behaviour is observed. The goal is to detect any signs of turbidity, liquid crystal formation, or phase separation. The proportions of each component in the formulation are determined through this aqueous titration, and subsequently, a ternary plot is generated. This plot aids in identifying distinct regions indicative of various phase behaviour outcomes.

2.5. Preparation of NAP-loaded NE

The NE was formulated using a S_{mix} consisting of Tween80 : PEG-400 in variable ratios, namely 1 : 0, 1 : 1, 2 : 1, 3 : 1, and 4 : 1. The oil phase and S_{mix} were subsequently combined at weight ratios of 1 : 9, 2 : 8(1 : 4), 3 : 7(1 : 2.3), 4 : 6 (1 : 1.5), 5 : 5(1 : 1), 6 : 4(1 : 0.7), 7 : 3(1 : 0.43), 8 : 2(1 : 0.25), 9 : 1 (1 : 0.1), 1 : 2, 1 : 3, 1 : 3.5, 1 : 5, 1 : 6, 1 : 7, and 1 : 8 (w/w), covering a wide range for the study. The NEs were prepared through the phase titration method. NAP was dissolved in GO (oil phase). Subsequently, S_{mix} was added while continuously stirring at an optimized speed. Distilled water was then added dropwise under moderate agitation, with process variables optimized to achieve a desirable mean droplet size. The formulation was visually assessed and confirmed as NEs based on transparency, flowability and clarity. Different NE parameters were then evaluated.

2.6. Development and optimization of NAP-GO-loaded NE using the Box–Behnken design (BBD)

The dependent variables of the formulation development included particle size, PDI, and zeta potential. Meanwhile, crucial independent factors such as oil concentration, surfactant concentration, and stirring speed were identified as influential parameters. Utilizing the Box–Behnken design (BBD), 15 combinations with independent factors were formulated, thus the resulting impact on the dependent variables was documented. These data were then put into Design-Expert (version 12 Stat Ease software) to construct a design model capable of accurately forecasting the optimized formulation. Subsequently, the formulation optimized by BBD was prepared.[23]

2.7. Characterization of optimized NE

2.7.1 Particle size and polydispersity index (PDI). Dynamic light scattering (DLS) was used to determine the mean particle size and distribution of particles in the formulated NE at room temperature. A Malvern Zeta Sizer Nano ZS from Malvern Instruments in the UK was utilized for this purpose. The NE mixture, with an average viscosity of 0.8860 cP and a refractive index of 1.452, was dispersed in distilled water. All measurements, including monitoring particle size distribution and PDI, were carried out in triplicate.[24]

2.7.2. Zeta potential. The zeta potential of the optimized formulation was evaluated using a Malvern Zetasizer (Nano-ZS, Malvern, UK). Initially, NE was diluted with Milli-Q water, and then the sample was filled to the specified mark in the sample chamber for analysis. All measurements were performed in triplicate.[25]

2.7.3. Morphology of the NE by transmission electron microscopy (TEM). The morphology of the prepared NE was analysed using TEM with a CRYO-TEM (TALOS S) of TECNAI G2 20 HR-TEM; (200 kV) FEI, U.S.A, operating at 200 kV and 9900× magnification. Approximately 50 µl of the NE was appropriately diluted with water and stained for 30 seconds using 1% w/v phosphotungstic acid. The stained sample was then dried on a coated copper grid. Two randomly created grids were observed for each sample.[26]

2.8. Preparation of the NE gel

Carbopol 974 (0.5%–1.5%) was carefully weighed and dispersed in Milli Q water for two hours. Then the drug loaded NE was added slowly to the Carbopol solution while being continuously stirred at 750 rpm and kept at 60 ± 2 °C to prevent excess air from getting trapped. Triethanolamine (0.056%) was then added dropwise to the mixture to neutralise it until the gel was formed. Following preparation, the NEG formulations were examined for consistency, viscosity, colour, and appearance.[27]

2.9. Evaluation of NEG

2.9.1. Homogeneity. The formulated gel was visually examined for homogeneity after being placed in the container. It was checked for the presence of any aggregates and their appearance.[26]

2.9.2. pH evaluation. 1 g of NEG formulation was carefully weighed and the pH meter electrode (Decibel DB-1011 Meter, Italy) was immersed into the formulation and allowed to attain equilibrium for 1 min before being used to measure pH.[28]

2.9.3. Texture analysis. The Texture Analyzer (TA.XTPlus) from Stable Micro Systems Ltd, Surrey, UK, was utilized for conducting texture analysis on the optimized gel. About 20 ml of the gel formulation was placed in a standard 100 mL beaker to ensure the exclusion of air producing a top surface that is smooth. A disc with a 40 mm diameter compressed the gel and was subsequently withdrawn. Method parameters, including speed and distance (implantation depth) were picked according to the type of gel. Three replicate analyses were carried out for each formulation at room temperature, maintaining consistent conditions for each measurement. Gel parameters, such as firmness, consistency, cohesiveness, and work of cohesion, were calculated from the force–time plot. The highest force, representing the firmness or the hardness of the prepared gel, and cohesiveness, indicating the work needed to get the gel deformed during the probe's descendant motion, were determined.[26]

2.9.4. Rheological study. An Anton Parr controlled stress rheometer (Physica MCR 101 Anton Parr Rheometer) was used to analyse the rheological characteristics of the gels. With the use of oscillating tests and flow experiments, the mechanical characteristics of NEG were studied. The rheometer's mechanical spectra were recorded at frequencies ranging from 0.01 to 10 Hz. Stress sweep tests were used to evaluate the viscoelastic

area at 1 Hz at 25 °C and 1 °C, all samples were examined using spindle number CP-50.[26]

2.10. *In vitro* drug release profile

The *in vitro* drug release study was conducted with the help of a dialysis cellulose membrane. Initially, the membrane underwent activation to open its pores, involving several steps: glycerol elimination was achieved by overnight washing under running water. Subsequently, it underwent treatment for 1 minute at 80 °C with a 0.3% w/v sodium sulphide solution in water to eliminate sulphur compounds. A two-minute hot water wash at 60 °C was followed by acidification using a 0.2% (v/v) sulfuric acid solution, and a subsequent rinse to remove the acid. Concurrently, 500 ml of phosphate buffer of pH 7.4 was prepared. The dialysis bag was soaked in dissolution media (release media) for 12 hours prior to usage. The formulations were placed in the dialysis bag before being dipped in 100 ml of the release medium kept in a beaker. The beaker was shaken in an incubator shaker at a speed of 200 rpm and at a temperature of 37 °C. To maintain the sink conditions, 3 ml aliquots of the sample were taken at predefined intervals (0.5, 1, 2, 4, 6, 8, and 24 h) and replaced with an equivalent volume of buffer. A UV spectrophotometer was used to analyze aliquots of NAP at 232 nm in a triplicate mode. For all the formulations *i.e.* NE and NEG the *in vitro* release graph and cumulative percent release graph were displayed in different models to find the best fit and compared with the conventional formulation (marketed as naproxen gel). Release kinetic modelling involved fitting the *in vitro* release data into various release kinetics models, including zero-order, first-order, Hixon–Crowell, Higuchi, and Korsmeyer–Peppas models. The model with the highest correlation coefficient value was deemed the most appropriate and considered the best-fit model.[29]

2.11. *Ex vivo* permeation study

The abdominal skin was removed from a Wistar rat after it was put to sleep using ether anesthesia. An electrical clipper was used to remove any hair from the animal's skin, subcutaneous tissues were surgically removed, and isopropyl alcohol was used to clean away any leftover sticking fat on the dermis side of the animal. 1 cm^2 of rat skin was cut out and positioned on top of the receptor compartment which was filled with PBS 7.4 (9 ml in this case). About 1 mL of NE and 1 g NEG and 1 g of conventional gel were appropriately filled in the donor compartment of different Franz diffusion cells. The diffusion cell was sealed completely using a paraffin film. The whole system was kept on a magnetic stirrer maintained at 37 ± 1 °C and 100 rpm for 24 hours. At fixed intervals of time (0, 1, 2, 4, 8, 12, 18, and 24 h), a 0.5 ml drug sample was taken out and substituted with an equal volume of freshly prepared media. The amount of drug in the sample was analyzed with a UV spectrophotometer at a wavelength of 232 nm.[30]

2.12. Confocal laser scanning microscopy (CLSM)

CLSM was employed to assess the range and depth of the formulation's penetration into the skin by a comparative analysis between rhodamine B solution, rhodamine B loaded NE and rhodamine loaded NEG. A conventional gel (marketed as naproxen gel) was also prepared by incorporating the same dye. Rat skin sections were placed on the Franz diffusion cell in separate donor compartments, one gram of NEG, an equivalent amount of NE containing the rhodamine B and rhodamine B solution was added on the doner compartment of the skin, and wrapped with a parafilm to stop evaporation and contamination. The setup was maintained at 37 ± 0.5 °C for eight hours while being continuously stirred. Afterward, the skin was removed, excess formulation was washed away, and the challenging step of infiltration through the stratum corneum, a barrier in topical drug delivery, was addressed. Once the formulation traversed the stratum corneum, absorption through deeper dermal layers becomes easier.[31] The skin underwent segmentation, stabilization, and examination through CLSM (Olympus Fluo View FV1000, Hamburg, Germany) employing an argon laser with excitation at 540 nm and emission at 625 nm. Subsequently, the formulations and the intermediate were assessed and compared based on their intensity and penetration depth.[28,32]

2.13. Stability study

The evaluation of formulation stability is a crucial aspect, and in this study, to evaluate the stable formulation, the NE and NEG were stored at a temperature of 25 °C ± 0.5 °C for a duration of 4 weeks. The stability evaluation focused on measuring variations in size, PDI, and amount of drug. The study was conducted four times at intervals of 0, 1, 2, 3, and 6 months.[33]

2.14. Safety assessment through the skin irritation study and histopathological analysis

To assess the safety of the gel, a skin irritation test was conducted. Wistar rats were chosen for the study, and patch testing was carried out on the intact skin of the animals to evaluate the irritation potential of both the NE and the optimized NEG formulations. All animal procedures were performed in accordance with the Guidelines for Care and Use of Laboratory Animals of Jamia Hamdard University and approved by the Animal Ethics Committee of Jamia Hamdard under registration number 173/GO/RE/S/2000/CPCSEA. The rats were housed in a controlled laboratory environment at a temperature of 25 °C ± 1 °C and relative humidity of 55% ± 5%. Rats, each with a cleaned dorsal hair area of 1 cm^2, were divided into three groups: the control group, the NEG group, and the conventional gel (marketed as naproxen gel) group, each consisting of three animals (n = 3). These animals were compared with an animal that had induced irritation. The rats were housed in a controlled laboratory environment at a temperature of 25 °C ± 1 °C and relative humidity of 55% ± 5%. Furthermore, a concentration of 20 mg mL^{-1} of NE and 250 mg of the optimized NEG (equivalent to 20 mg of NA) were

uniformly applied to the shaved skin of the rats three times daily in divided doses. The skin was examined for any visible changes at 24, 48, and 72 hours and scored accordingly. The degree of erythema was evaluated using a scale ranging from 0 to 4, where 0, 1, 2, 3, and 4 represented no, slight, moderate, and moderate to severe, and severe erythema, respectively.[26] After the pharmacodynamic study, the right knee joint was surgically removed and immersed in 10% formalin for 24 hours at a temperature of 40 °C. Afterward, decalcification of the joint was carried out using a 5% HCl solution (Sigma Aldrich) for a duration of 4 days at 40 °C. To prepare the joint for histological examination, the specimens were subjected to dehydration using acetone and then embedded in paraffin following the decalcification process. The paraffin-embedded right knee joints were sliced along the sagittal axis into sections that are 5 μm thick. These sections were subjected to staining with Hematoxylin and Eosin (H&E) to visualize and confirm any changes in the synovial membrane and cartilage within the knee joint.[34]

3. Results and discussion

3.1. Screening of NE ingredients

The formulation ingredients selected for development were all of pharmaceutical standard. The inclusion of both the surfactant and cosurfactant in this formulation was anticipated to enhance skin permeation and improve nano-emulsification, as outlined in ref. 21. Ensuring the drug's complete solubility in the chosen oil phase is crucial for maintaining NE stability as shown in the ESI, Table S1.† This characteristic becomes especially advantageous due to the higher concentration gradient, leading to an increased therapeutic effect by augmenting percutaneous drug permeation. The solubility of NAP was notably high in GO (>5mg ml^{-1}), making it a potential candidate for anti-inflammatory topical applications, traditionally used to alleviate pain and inflammation in ancient medicinal practices. The selected surfactant needs to effectively lower interfacial tension to facilitate fine dispersion, creating a flexible film that can envelop droplets with ease. Moreover, the surfactant should possess the right lipophilic attributes to achieve an optimal interface curvature. In comparison to different nonionic surfactants such as Cremophor and Tween 80, it was observed that Tween 80 exhibited the highest emulsification capacity for the designated oil phase as shown in Table S1.† However, achieving the desired interfacial area isn't always attainable with just one surfactant. This is where the cosurfactant becomes pivotal, enhancing the overall stability of the NE. The selection of cosurfactants was guided by the results obtained from the phase behaviour study, with the NE area in the phase diagram indicating the potential emulsification effectiveness of the chosen surfactant system, as discussed in ref. 21.

The tried cosurfactants were ethanol, PEG 400, and propylene glycol. PEG 400 demonstrated superior emulsification capabilities for the specific oil and surfactant combination, as evidenced by insights from the phase diagram analysis. It's worth noting that due to regulatory constraints, ethanol, despite its efficacy, was not included in the NE formulation design, as per the mentioned reference.[21]

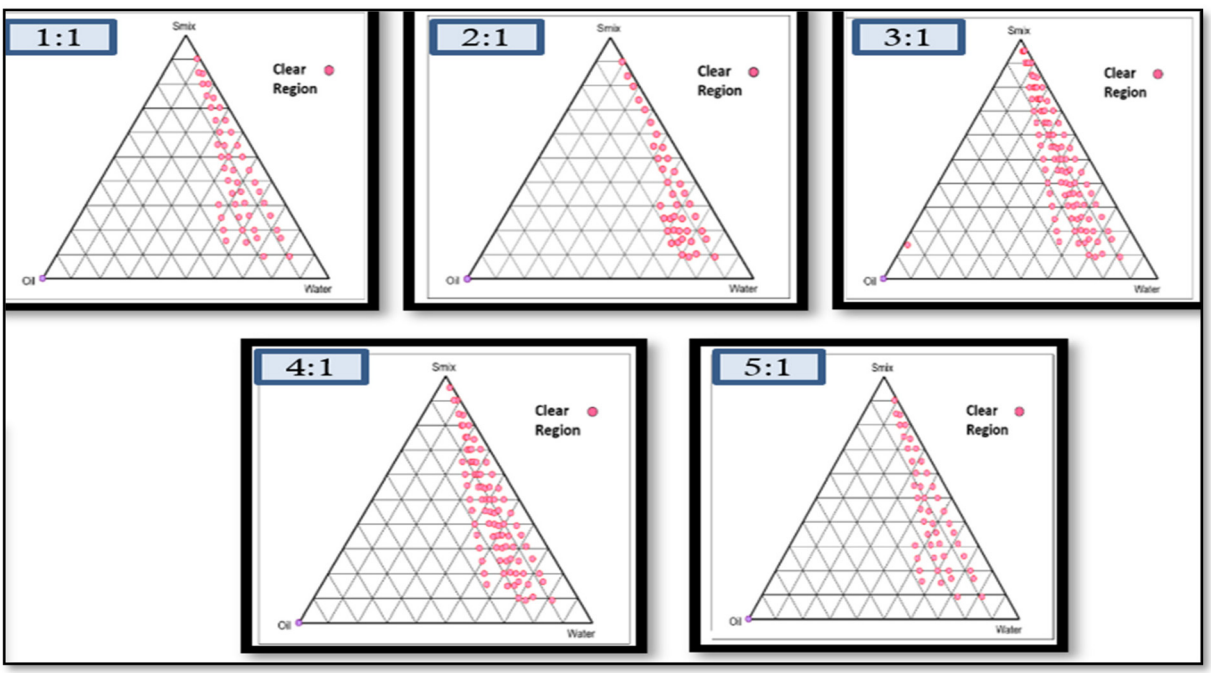

Fig. 1 Pseudo ternary phase diagram using the aqueous titration method showing an o/w NE region for 1 : 1, 2 : 1, 3 : 1 and 4 : 1 S_{mix} of Tween-80 to PEG-400.

3.2. Development of pseudo-ternary phase diagrams

To ascertain the concentrations of various components within the current boundary of NEs, a pseudo-ternary phase diagram was prepared using an aqueous titration method. The phase diagram was developed by varying the S_{mix} ratio of Tween-80 to PEG-400, namely 1 : 1, 2 : 1, 3 : 1, and 4 : 1 as shown in Fig. 1. A pseudo-ternary phase diagram serves as a tool to define the optimal composition range for excipients and is employed in designing the NE area. This technique illustrates the influence of volume changes in different phases on the system's behaviour.[35] Analysis of the diagram revealed that among the ratios 1 : 1, 2 : 1, 3 : 1, and 4 : 1, the pseudo-ternary phase diagram displays the o/w NE region. The 3 : 1 S_{mix} ratio covered the highest possible area, and was thus chosen for subsequent investigations. The size of the NE region, whether small or large, relies on the ability of the specific surfactant or surfactant blend to solubilize the oil phase. Greater solubilisation results in a larger area with a clearer, homogeneous solution.

The pseudo-ternary phase diagram serves as a tool to define the ideal composition range for excipients and is a technique employed in designing the NE area. This method illustrates the impact of volume changes in different phases on the system's behaviour.[35]

3.3. Development and optimization of NAP-loaded NE using the Box–Behnken design (BBD)

The three-factor, three-level Box–Behnken design was used. Fifteen runs for NAP-loaded NE formulations were produced and analyzed using the design software as mentioned in Table 1, which mentioned the independent parameters; oil concentration (A), surfactant concentration (B), and stirring speed (C), as well as the dependent responses particle size (R_1), PDI (R_2), and zeta potential (R_3). NE was prepared using the aqueous titration method and the runs were generated using the BBD. The summary of regression analysis and findings for responses of R_1, R_2 and R_3 for quadratic equation fitting have been given in Table S2.†

3.3.1. Effects of independent variables on the particle size. The NE formulations ranged in size from 96.0 nm to 266.0 nm. The particle size distribution has been determined using dynamic light scattering. The effects of independent factors on size are shown in the response surface graph depicted in Fig. 2. From the response surface graph it was observed that with the increase in the stirring speed and surfactant concentration, the particle size decreased whereas the increase in oil concentration caused a considerable increase in particle size.[18]

3.3.2. Effects of independent variables on the PDI. PDI levels were found to be in between 0.107 and 0.349. The influence of numerous independent factors on PDI is depicted in 3D graphics in Fig. 3. In the case of an increase in the oil concentration the value of PDI increases, however, an increase in the surfactant concentration and stirring speed decreases the value of PDI significantly.

3.3.3. Effects of independent variables on the zeta potential. The zeta potential of the NE formulations ranged from −23.8 to −26.5 mV. The zeta potential of NE increases as the oil concentration increases while the zeta potential of NE decreases as the surfactant concentration increases. There was no such variation noticed with the change in the stirring speed as depicted in Fig. 4.

Table 1 Box–Behnken design factors for NE preparation

Factors Independent variables	Levels Low	 High
A = oil concentration (%v/v)	1	3
B = surfactant concentration (%v/v)	4	18
C = stirring speed (rpm)	300	1000

Dependent variables: R_1 = particle size (nm), R_2 = PDI, R_3 = zeta potential (mV).

3.4. Characterization of optimized NE formulation

3.4.1. Particle size and polydispersity index (PDI). It was observed that the optimized NE produced by aqueous titration contained particles in the nanometer range. *i.e.*, 209.2 nm. A specific formulation's size distribution of scattered particles is indicated by the PDI which in the case of given trials ranges

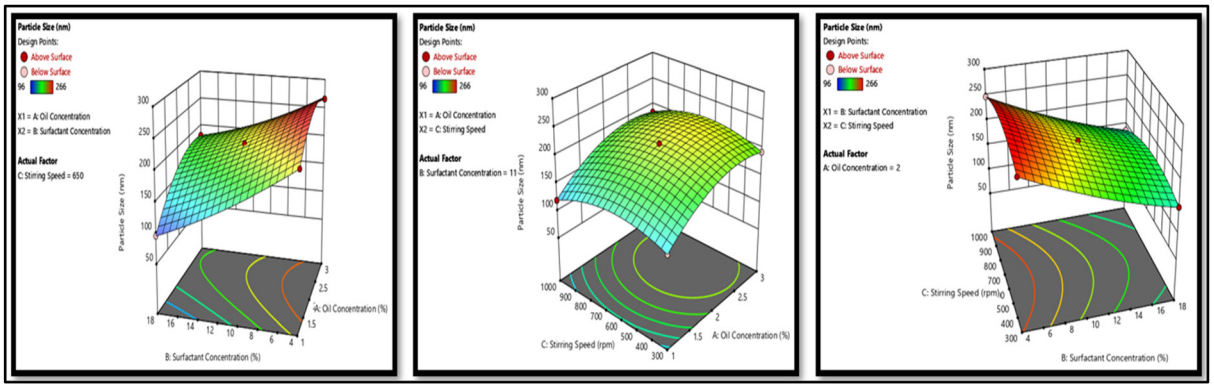

Fig. 2 Response surface plots of the factorial design show how the independent variables affect the variables dependent on the particle size.

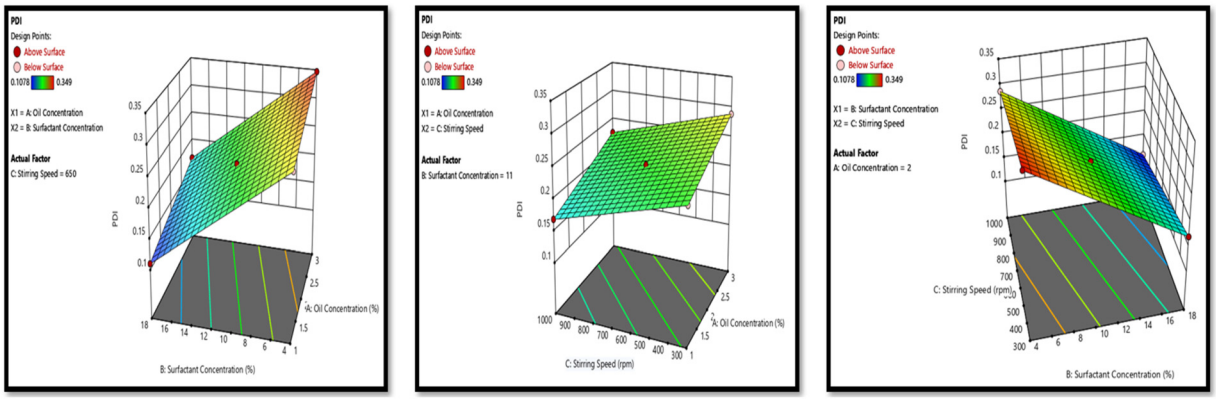

Fig. 3 Response surface plots of the factorial design show how the independent variables affect the variables dependent on PDI.

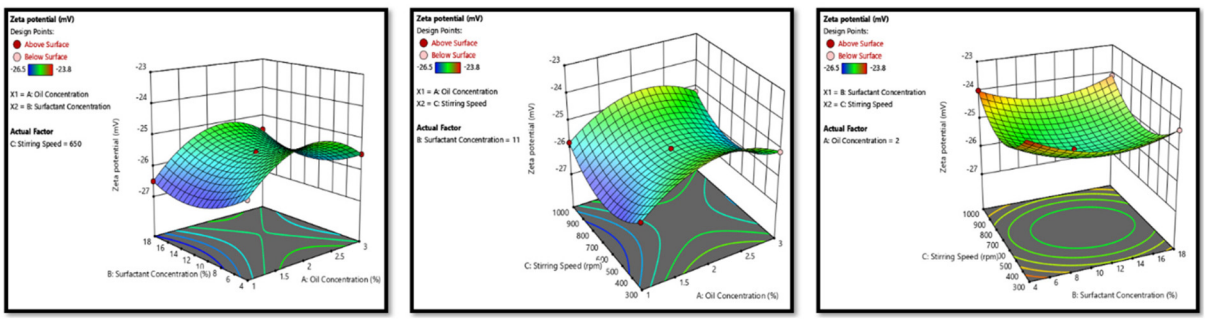

Fig. 4 Response surface plots of the factorial design show how the independent variables affect the variables dependent on the zeta potential.

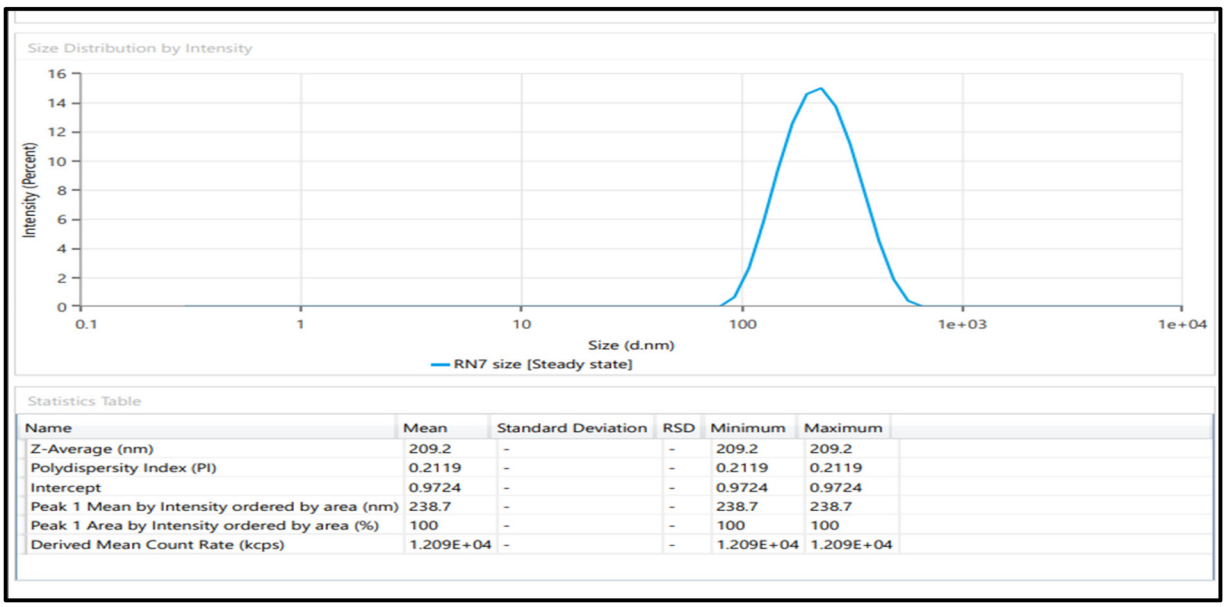

Fig. 5 Particle size (nm) and PDI of the optimized drug loaded NE.

within the limit of 0.1 to 0.3. The PDI value more than 0.4 shows a wide distribution of size and a value between 0.10 and 0.40 denotes a considerably polydisperse system.[24] The optimized NE's PDI turned out to be 0.2119 as given in Fig. 5. This range is indicative of neither broad nor very narrow, thus it is concluded that optimized NE represents an acceptable polydisperse system. The optimized NE's PDI turned out to be 0.2119 as given in Fig. 5. This range is indicative of neither

penetration through skin(25).

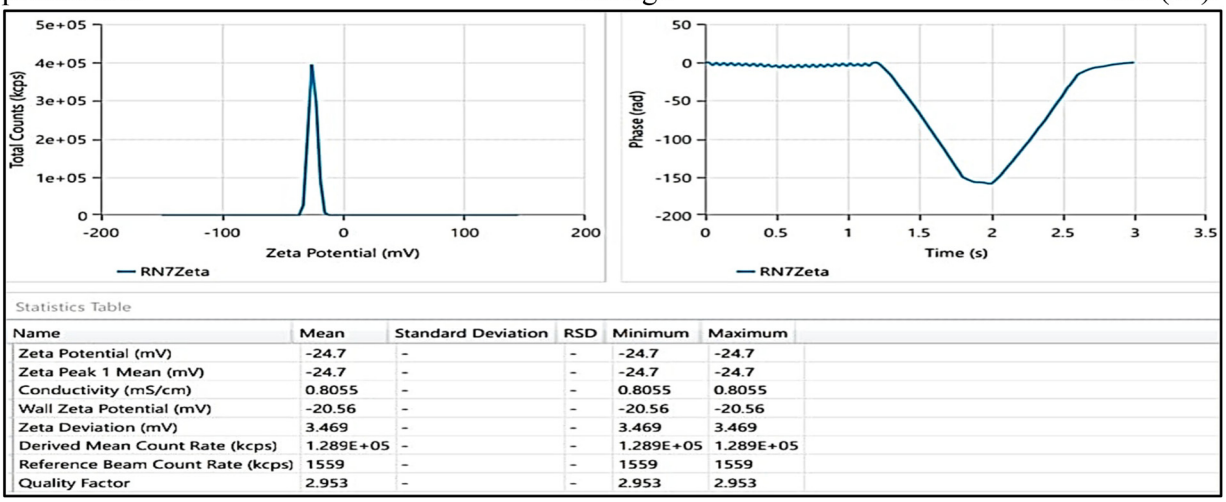

Statistics Table

Name	Mean	Standard Deviation	RSD	Minimum	Maximum
Zeta Potential (mV)	-24.7	-	-	-24.7	-24.7
Zeta Peak 1 Mean (mV)	-24.7	-	-	-24.7	-24.7
Conductivity (mS/cm)	0.8055	-	-	0.8055	0.8055
Wall Zeta Potential (mV)	-20.56	-	-	-20.56	-20.56
Zeta Deviation (mV)	3.469	-	-	3.469	3.469
Derived Mean Count Rate (kcps)	1.289E+05	-	-	1.289E+05	1.289E+05
Reference Beam Count Rate (kcps)	1559	-	-	1559	1559
Quality Factor	2.953	-	-	2.953	2.953

Fig. 6 Zeta potential (mv) of optimized drug loaded NE was a negative value of −24.7 mV.

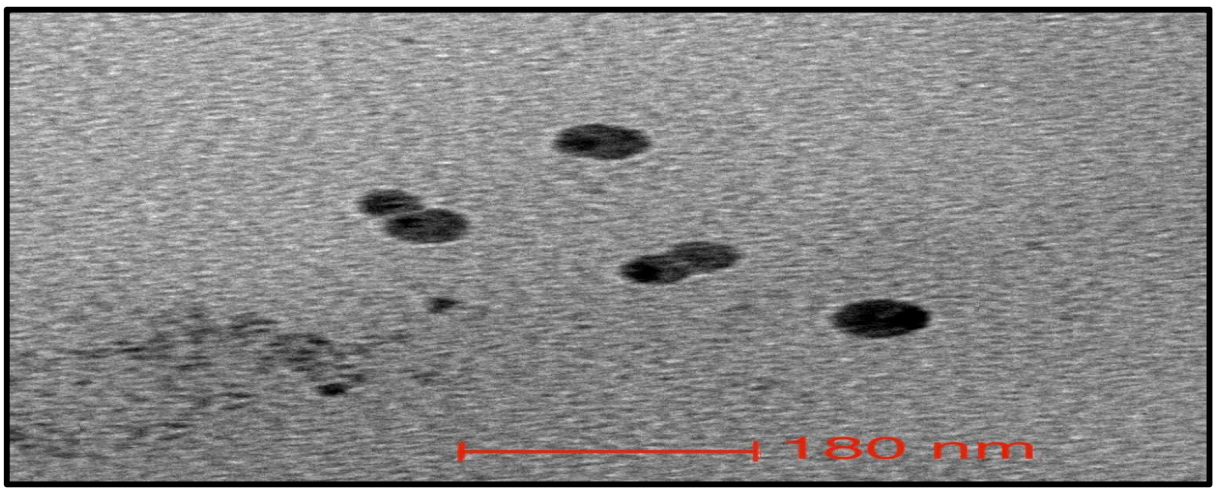

Fig. 7 Transmission electron microscopy image of drug loaded NE.

broad nor narrow, thus it is concluded that optimized NE represents an approximate polydisperse system.

3.4.2. Zeta potential. An effective method for assessing a distributed system's stability is zeta potential analysis. This gives us an insight into particle aggregation due to electrostatic repulsion.[36]Non-ionic surfactants were the surfactant of choice for NE preparation, the reason being the benefits they offer in terms of stability, compatibility, less toxicity, and non-irritability as compared to amphoteric or ionic surfactants.[24] The optimized NE has a zeta potential of −24.7 mV and a negative value (Fig. 6), which indicate good formulation stability and prevent it from coagulating and provide an electrostatically stable nanoemulsion and the negative zeta potential increases transdermal penetration through the skin.[25]

3.4.3. Morphology/transmission electron microscopy (TEM). The NE was further characterized using TEM analysis which showed a slightly spherical structure with ranges between 180 and 200 nm (Fig. 7). The size that the Malvern Zetasizer produced was somewhat smaller than this one. This variation in particle size might be the result of different sample preparation methods and principles of analytical techniques used in the two approaches.

Table 2 Texture observations of different NEG formulations

Formulation	Carbopol (% w/v)	pH	Homogeneity	Spreadability
$NEG_{0.5}$	0.5	6.3 ± 0.29	Good	Watery
$NEG_{0.75}$	0.75	6.4 ± 0.21	Good	Watery
NEG_{1}	1	6.4 ± 0.18	Good	Watery
$NEG_{1.5}$	**1.5**	**6.4 ± 0.32**	**Good**	**Good**

3.5. Preparation of NE loaded gel

NEGs were prepared by adding Carbopol-974 (0.5% to 1.5% w/v) as a gelling agent as given in Table 2. The table gives the details of different batches of Carbopol-974. The gel with 1.5% w/v Carbopol ($NEG_{1.5}$) was found to be the most suitable and stable formulation, considering the consistency, spreadability and texture but the gel became extremely fluid below this Carbopol-974 concentration and hardened above this concentration. To the final optimized gel formulation glycerin (1%v/v) was added as a humectant and methyl paraben (0.02% w/v) as a preservative. It was then characterized on the basis of several gel assessment criteria.

Table 3 Texture analysis report of the optimized NEG's

S. No	Parameters (mean ± SD) (n = 3)	Values
1	Spreadability (cm)	6.8 ± 0.127 (easily spreadable)
2	Homogeneity	Smooth texture (no grittiness was found)
3	Extrudability (g cm^{-2})	1.7 ± 0.32

3.6. Evaluation of the optimized nano-emulsion gel (NEG)

3.6.1 Spreadability and extrudability. The spreadability of the final optimized gel was observed to be 6.8 ± 0.127 cm in diameter exhibiting the gel's simple spreadability. Characterization of the gel was further carried out to assess the various parameters of the prepared gel as mentioned in Table 3.

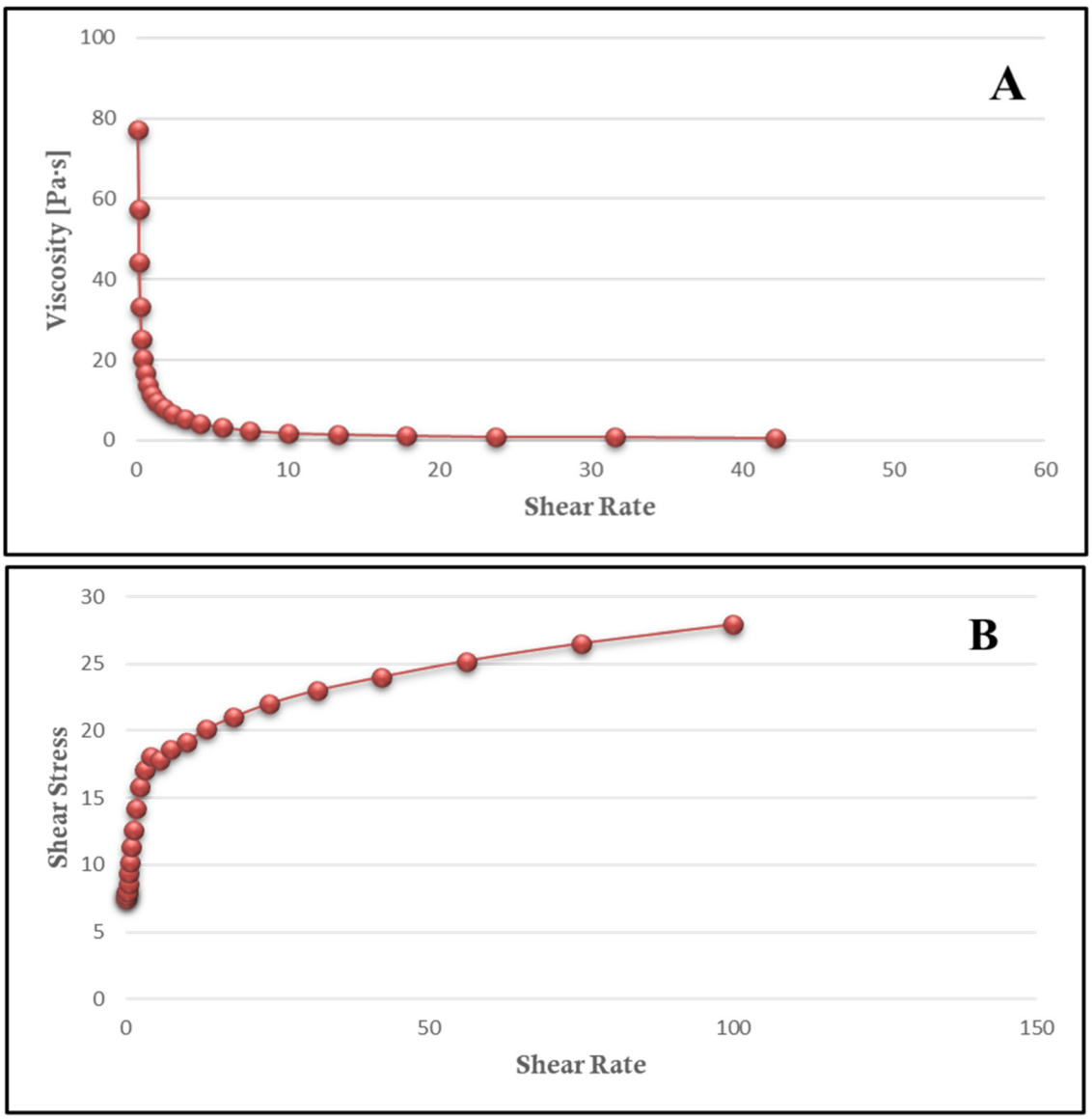

Fig. 8 Gel rheological measurements with the help of a rheometer at 25 °C with variations in the (a) viscosity; (b) shear stress with respect to the change in the shear rate.

3.6.2. pH and homogeneity. The optimized formulation's pH value turned out to be 6.8 ± 0.24 and the texture of the gel was found to be consistent, smooth, and grittiness free.

3.6.3. Rheological behavior studies. The viscosity of the formulated NEG was discovered to be 44.6 Pa s. Fig. 8a and b show the variance in NEG's fluidity and stress caused by shear. It is evident from the image below that the viscosities of NEG dropped as the rate of shear was impacted from 0.1 s^{-1} to 100 s^{-1} indicating that it functioned as a shear thinning (non-Newtonian) pseudoplastic fluid. Because of the reduced viscosities at a higher shear rate, the flow behavior may be controlled with less energy. Additionally, the NEG was shown to exhibit superior thixotropic capabilities, opening the door to potential industrial applications. Additionally, as the NEG was sheared, the polymer network was disrupted and microscopic gel layers moved upon the adjacent layer, suggesting an increase in shear stress. These figures show the overall shear-thinning behavior of the gel.[26]

3.6.4. Texture analysis of NEG. The gel formulation is characterized by properties *viz* mechanical attributes that include cohesion, firmness, consistency, and viscosity index. These are the properties which impact patient compliance and application. The gel's stickiness is assessed by its viscosity

Table 4 Texture analysis data depicting the values of firmness, consistency, cohesiveness and work of cohesion of NEG

Firmness (g)	Consistency (g s^{-1})	Cohesiveness (g)	Work of cohesion (g s^{-1})
Force 1	Area F-T 1 : 2	Force 2	Area F-T 2 : 3
341.31	1357.08	−64.48	−1452.45
341.31	1357.08	−64.48	−1452.45
0.00	0.00	0.00	0.00
0.00	0.00	0.00	0.00

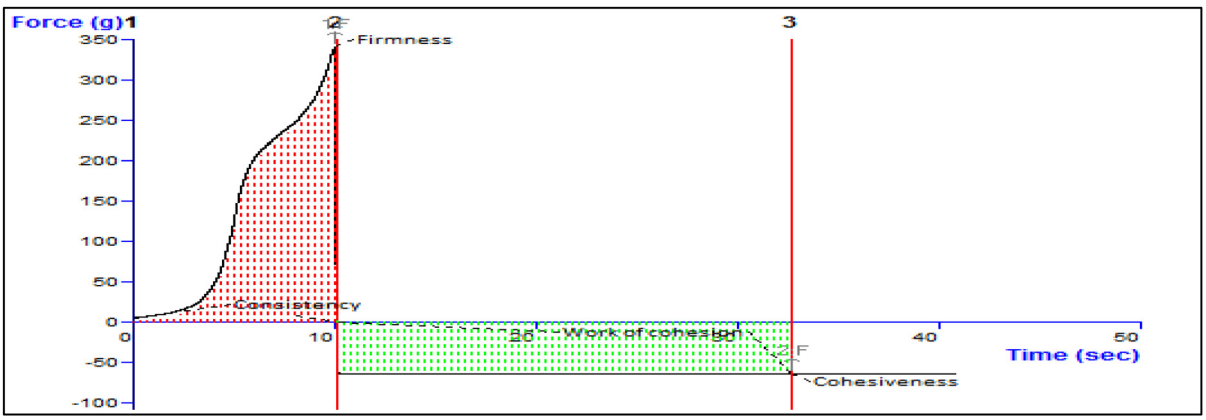

Fig. 9 Texture analysis data of the NAP loaded NEG. The force–time plot was used to calculate parameters such as firmness, consistency, cohesiveness, and work of cohesion. The maximum positive force represents the hardness/firmness of the gel whereas cohesiveness is described as the negative area under the force–time curve.

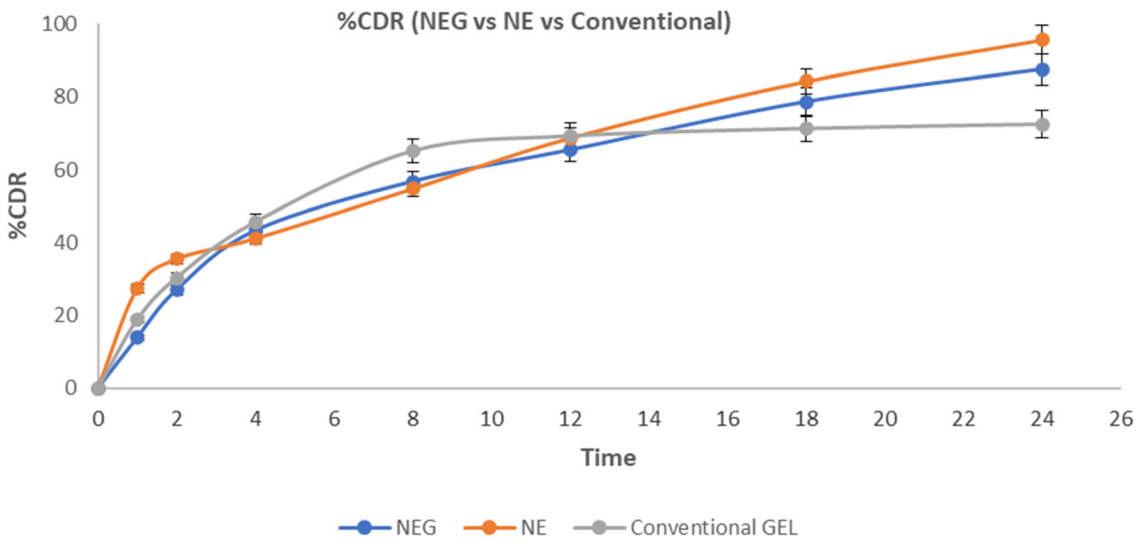

Fig. 10 Comparative result of %CDR of NEG, NE and conventional gel (*in vitro*).

index, and its strength can be measured by its hardness. The higher the value, the better the strength of the gel. The optimized cohesion, viscosity index, hardness, and consistency values of NEG were found to be 341.31 g, 1357.08 g s^{-1}, −64.48 g and 1452.45 g s^{-1}, respectively as shown in Table 4 and the graph is shown in Fig. 9. Each characteristic of the gel was found to be indeed present in the optimized NEG.[34]

3.7. *In vitro* drug release study

In vitro drug release study plays a crucial role in the performance of the formulation in terms of drug available using a selected carrier system. Graphical plots between the time interval and cumulative percentage of drug release have been shown in Fig. 10. The drug release rates for NEG, NE, and conventional gel (marketed as naproxen gel) were determined.

The release kinetics data revealed distinct patterns among the formulations. NE exhibited a release of 95.64 ± 0.79% within 24 h, whereas NEG demonstrated a slower release of 87.44 ± 0.84%. This discrepancy can be attributed to the three-dimensional firm structure of the NEG. In contrast, the conventional gel displayed a release of 30.28 ± 1.55% within 2 h. The release profiles of both NEG and NE conformed to the Higuchi model, as indicated by the coefficient of regression close to 1.0. On the other hand, the conventional gel (marketed as naproxen gel) followed a Peppas–Korsmeyer release pattern.

3.8. *Ex vivo* skin permeation study

The permeation of the drug from both NEG and NE formulations was monitored for a duration of 24 h and found to be 9.3287 μg cm^{-2} and 17.447 μg cm^{-2}. A graph was constructed, illustrating the relationship between the cumulative release per cm^2 (μg cm^{-2}) and time as depicted in Fig. 11. These release data were then utilized to determine the steady flux

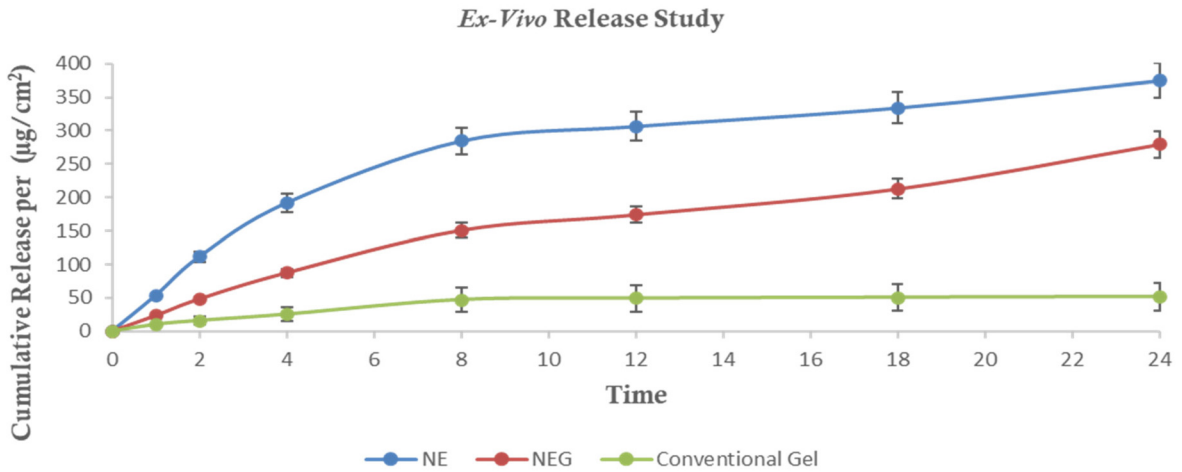

Fig. 11 Comparative result of cumulative release (per (μg cm^{-2}) of NE, NEG and conventional gel (*Ex vivo*).

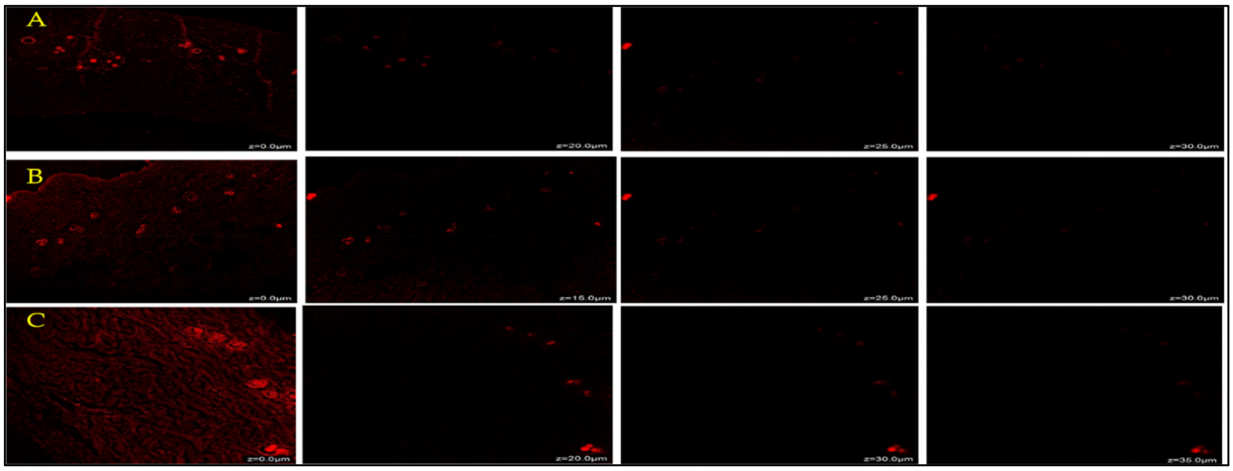

Fig. 12 CLMS comparison of rhodamine penetration between (A) rhodamine loaded conventional gel, (B) rhodamine loaded NEG and (C) rhodamine loaded NE through animal skin tissue.

and permeation coefficient values for NEG, NE and conventional gel.

During a 24-hour period, the total drug release through the rat skin was found to be 73.40 ± 0.96%, 54.72 ± 1.97%, and 10.04 ± 1.87% for the NE, NEG, and conventional gel, respectively. Flux refers to the amount of drug that permeates through a selected membrane per unit time. The steady flux occurs after the initial lag phase when the permeation rate becomes constant. For the NE, NEG, and conventional gel, the flux values were calculated to be 17.447 μg cm^{-2} h^{-1}, 9.3287 μg cm^{-2} h^{-1}, and 2.937 μg cm^{-2} h^{-1}, respectively. The permeation coefficient was determined by dividing the flux by the entire quantity of the drug in the donor compartment (5000 μg NAP). The permeation coefficients for the NE, NEG, and conventional gel were calculated as 0.0343, 0.01856, and 0.005874, respectively.

The NEG having a higher permeation coefficient and flux indicated its greater permeation into the skin compared to the conventional gel. This enhanced permeation is beneficial for the treatment of OA.

Table 5 Stability parameters of NEG

Parameter	Initial	1st month	2nd month	3rd month	6th month
Size (nm)	209.2	211.5	214.2	217.1	218.5
PDI	0.2119	0.2298	0.2414	0.2638	0.2851
Drug content (%)	98.5	98.2	97.4	97.1	96.6

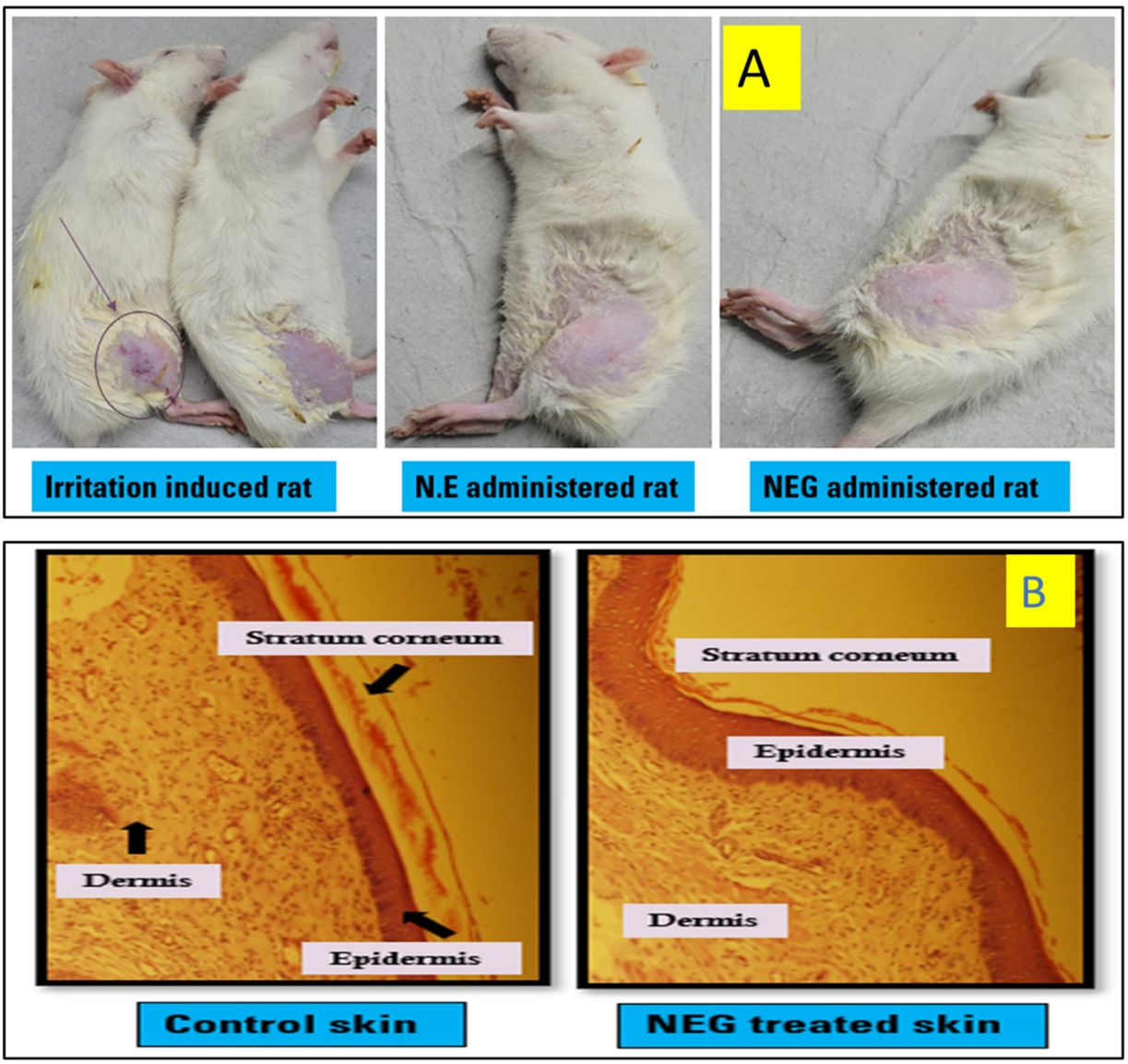

Fig. 13 (A) The skin irritation study of both untreated control skins and skins treated with NEG. The control skin shows an integral stratum corneum (SC) with clearly defined boundaries. No signs of inflamed cells were observed in the dermis. The collagen fiber bundle was well packed, and the skin's appendages seemed ordinary. (B) Histopathological examination of NEG.

3.9. Confocal laser scanning microscopy (CLSM)

Fig. 12 shows the extent of penetration of rhodamine B conventional gel (marketed as naproxen gel), NE and NEG formulations at different rates *via* skin. According to the fluorescence intensities, the rhodamine B loaded nanoemulgel easily penetrated the deeper layers of the skin, up to 35 μm, whereas the drug loaded conventional gel only penetrated up to 25 μm. The presence of a high fluorescence signal from 10 m to 35 μm, which indicates the stratum corneum permeation of the formulation, is noteworthy. Therefore, due to the stratum corneum's thickness of 10 to 40 μm it is possible that a product passes through this area and penetrates deeper unaffected layers before being released *via* diffusion.[34]

3.10. Stability study

The particle size, polydispersity index, and drug content were monitored for NEG maintained at a temperature of 25 °C for a time span of 6 months, and the results are summed up in Table 5. NEG was shown to be quite stable, showing neither a decline in drug concentration nor a significant increase in size or PDI. This indicates that under ideal storage conditions, the NE and NEG formulations were able to retain their size without experiencing any drug loss or leaching.[26,37]

3.11. Safety assessment using the skin irritation study and histopathological analysis

Microscopic analysis was conducted on cross sections of both untreated control skins and skins treated with NEG. The control skin shows an integral stratum corneum (SC) with clearly defined boundaries, including the SC layer, epidermis, and dermis, as shown in Fig. 13a. No signs of inflamed cells were observed in the dermis. The collagen fiber bundle was well packed, and the skin's appendages seemed ordinary.

However, in the case of skins treated with NEG for a duration of 6 hours, notable changes were evident in the SC morphology (Fig. 13b). The surface of the SC was weakened, causing the layers of the treated skin to be unevenly knitted together. This change might be due to the presence of surfactants, which are known to eliminate intercellular lipids and sever keratinocyte desmosome connections.[34,37] Additionally, the presence of the formulation within the epidermis led to increased intercellular spaces and noticeable gaps. Moreover, abnormal separation of collagen bundles in the dermis was observed. These observations suggest that the NE from the gel was permeating the skin, disturbing the overall structure of the skin barrier, and extracting intercellular lipids. These factors might explain the observed histological alterations.

The histological assessments indicated the absence of damaged cells in the dermis, indicating that the application of NEG was not causing any topical inflammation or irritation. This suggests that the use of the NEG was safe for topical application.[34]

4. Conclusion

The development of a novel formulation, NEG incorporating NAP in GO holds promise for addressing the symptoms of OA. By combining NAP with GO, known for their efficacy in managing OA symptoms, this formulation is expected to exhibit synergistic effects. Moreover, the nano-sized particles enhance patient compliance by potentially decreasing the frequency of dosage, presenting a convenient and effective treatment option for OA management. The limited treatment options further complicate the patient's situation. Therefore, the fabrication of a novel NEG incorporating NAP to target locoregionally through topical administration can ameliorate OA. It is anticipated that this combination will improve patient compliance.

Institutional review board statement

The study protocol was approved by the Jamia Hamdard Animal Ethics Committee (JHAEC, Registration No. 173/GO/RE/S/2000/CPCSEA, New Delhi, India).

Conflicts of interest

The authors declare no conflict of interest.

Acknowledgements

The authors are highly grateful to the Jamia Hamdard University, New Delhi, India for all its support.

References

1 D. Bhatia, T. Bejarano and M. Novo, Current interventions in the management of knee osteoarthritis, *J. Pharm. BioAllied Sci.*, 2013, **5**(1), 30–38.
2 M. K. Javaid and N. K. Arden, Bone and osteoarthritis: What is the relationship?, *Arthritis Rheum.*, 2013, **65**(6), 1418–1420.
3 S. M. Hussain, D. W. Neilly, S. Baliga, S. Patil and R. M. D. Meek, Knee osteoarthritis: A review of management options, *Scott. Med. J.*, 2016, **61**(1), 7–16.
4 M. Velangi, S. Mandalika, S. Shukla and V. Pradhan, Effect of Vitamin D3 and Virgin Coconut Oil on Cartilage Degeneration, Inflammation and Functional Abilities in Early Knee Osteoarthritis, *Funct. Foods Health Dis.*, 2019, **9**(10), 662.
5 R. Bitton, The economic burden of osteoarthritis, *Am. J. Manag. Care*, 2009, **44**(4), 865–867.
6 A. D. Woolf and B. Pfleger, Burden of major musculoskeletal conditions, *Bull. W. H. O.*, 2003, **81**(9), 646–656.
7 K. D. Allen, L. M. Thoma and Y. M. Golightly, Epidemiology of osteoarthritis, *Osteoarthrotic Cartilage*, 2022, **30**(2), 184–195.

8 T. Murakami, H. Higaki, Y. Sawae, N. Ohtsuki, S. Moriyama and Y. Nakanishi, Adaptive multimode lubrication in natural synovial joints and artificial joints, *Proc. Inst. Mech. Eng., Part H*, 1998, **212**(1), 23–35.
9 C. J. M. Bachmeier, L. M. March, M. J. Cross, H. M. Lapsley, K. L. Tribe, B. G. Courtenay, *et al.*, A comparison of outcomes in osteoarthritis patients undergoing total hip and knee replacement surgery, *Osteoarthrotic Cartilage*, 2001, **9**(2), 137–146.
10 M. Yang, X. Feng, J. Ding, F. Chang and X. Chen, Nanotherapeutics relieve rheumatoid arthritis, *J. Controlled Release*, 2017, **252**, 108–124.
11 M. K. Jeengar, S. V. K. Rompicharla, S. Shrivastava, N. Chella, N. R. Shastri, V. G. M. Naidu, *et al.*, Emu oil based nano-emulgel for topical delivery of curcumin, *Int. J. Pharm.*, 2016, **506**(1–2), 222–236.
12 N. Ustundag Okur, V. Yozgatlı, M. E. Okur, A. Yoltaş and P. I. Siafaka, Improving therapeutic efficacy of voriconazole against fungal keratitis: Thermo-sensitive in situ gels as ophthalmic drug carriers, *J. Drug Delivery Sci. Technol.*, 2019, **49**, 323–333.
13 N. Üstündağ Okur, Ş. Apaydin, N. Ü. Karabay Yavaşoğlu, A. Yavaşoglu and H. Y. Karasulu, Evaluation of skin permeation and anti-inflammatory and analgesic effects of new naproxen microemulsion formulations, *Int. J. Pharm.*, 2011, **416**(1), 136–144.
14 L. Binder, J. Jatschka, E. M. Kulovits, S. Seeböck, H. Kählig and C. Valenta, Simultaneous penetration monitoring of oil component and active drug from fluorinated nanoemulsions, *Int. J. Pharm.*, 2018, **552**(1–2), 312–318.
15 T. Uriah, S. Rai, J. P. Mohanty and P. Ghosh, Physicochemical evaluation, in vitro anti-inflammatory, in vitro anti-arthritic activities and GC-MS analysis of the oil from the leaves of Gaultheria fragrantissima Wall of Meghalaya, *J. Drug Delivery Ther.*, 2019, **9**(3 s), 170–180.
16 W. Zhang, M. Doherty, G. Peat, S. M. A. Bierma-Zeinstra, N. K. Arden, B. Bresnihan, *et al.*, EULAR evidence-based recommendations for the diagnosis of knee osteoarthritis, *Ann. Rheum. Dis.*, 2010, **69**(3), 483–489.
17 J. Ahmad, K. Kohli, S. R. Mir and S. Amin, Formulation of self-nanoemulsifying drug delivery system for telmisartan with improved dissolution and oral bioavailability, *J. Dispersion Sci. Technol.*, 2011, **32**(7), 958–968.
18 S. Kotta, A. W. Khan, S. H. Ansari, R. K. Sharma and J. Ali, Formulation of nanoemulsion: A comparison between phase inversion composition method and high-pressure homogenization method, *Drug Delivery*, 2015, **22**(4), 455–466.
19 J. Ahmad, S. R. Mir, K. Kohli and S. Amin, Quality by design approach for self nanoemulsifying system of paclitaxel, *Sci. Adv. Mater.*, 2014, **453**, 68–77.
20 S. Akhter, M. Anwar, M. A. Siddiqui, I. Ahmad, J. Ahmad, M. Z. Ahmad, *et al.*, Improving the topical ocular pharmacokinetics of an immunosuppressant agent with mucoadhesive nanoemulsions: Formulation development, *in vitro* and *in vivo* studies, *Colloids Surf., B*, 2016, **148**, 19–29.
21 S. D. Acharya, P. K. Tamane, S. N. Khante and V. B. Pokharkar, QbD based optimization of curcumin nanoemulsion: DoE and cytotoxicity studies, *Indian J. Pharm. Educ. Res.*, 2020, **54**, 329–336.
22 J. Ahmad, S. R. Mir, K. Kohli and S. Amin, Effect of oil and co-surfactant on the formation of Solutol HS 15 based colloidal drug carrier by Box-Behnken statistical design, *Colloids Surf., A*, 2014, **6**(8), 1778–1791.
23 J. Luan, F. Zheng, X. Yang, A. Yu and G. Zhai, Nanostructured lipid carriers for oral delivery of baicalin: In vitro and in vivo evaluation, *Colloids Surf., A*, 2015, **466**, 154–159.
24 S. Mohapatra, M. A. Mirza, S. Ahmad, U. Farooq, M. J. Ansari, K. Kohli, *et al.*, Quality by Design Assisted Optimization and Risk Assessment of Black Cohosh Loaded Ethosomal Gel for Menopause: Investigating Different Formulation and Process Variables, *Pharmaceutics*, 2023, **15**(2), 465.
25 F. Zakir, B. Vaidya, A. K. Goyal, B. Malik and S. P. Vyas, Development and characterization of oleic acid vesicles for the topical delivery of fluconazole, *Drug Delivery*, 2010, **17**(4), 238–248.
26 W. A. Mahdi, S. I. Bukhari, S. S. Imam, S. Alshehri, A. Zafar and M. Yasir, Formulation and optimization of butenafine-loaded topical nano lipid carrier-based gel: Characterization, irritation study, and anti-fungal activity, *Pharmaceutics*, 2021, **13**(7), 1087.
27 F. Zakir, A. Ahmad, U. Farooq, M. A. Mirza, A. Tripathi, D. Singh, *et al.*, Design and development of a commercially viable in situ nanoemulgel for the treatment of postmenopausal osteoporosis, *Nanomedicine*, 2020, **15**(12), 1167–1187.
28 A. Hardiansyah, M. C. Yang, T. Y. Liu, C. Y. Kuo, L. Y. Huang and T. Y. Chan, Hydrophobic Drug-Loaded PEGylated Magnetic Liposomes for Drug-Controlled Release, *Nanoscale Res. Lett.*, 2017, **12**, 1–1.
29 O. González-González, I. O. Ramirez, B. I. Ramirez, P. O'Connell, M. P. Ballesteros, J. J. Torrado, *et al.*, Drug Stability: ICH versus Accelerated Predictive Stability Studies, *Pharmaceutics*, 2022, **14**(11), 2324.
30 C. Orhan, M. Tuzcu, A. S. Durmus, N. Sahin, I. H. Ozercan, P. B. D. Deeh, *et al.*, Protective effect of a novel polyherbal formulation on experimentally induced osteoarthritis in a rat model, *Biomed. Pharmacother.*, 2022, **151**, 113052.
31 G. P. Kumar and P. Rajeshwarrao, Nonionic surfactant vesicular systems for effective drug delivery—an overview, *Acta Pharm. Sin. B*, 2011, **1**(4), 208–219.
32 G. A. Schellekens, H. Visser, B. A. W. De Jong, F. H. J. Van Den Hoogen, J. M. W. Hazes, F. C. Breedveld, *et al.*, The diagnostic properties of rheumatoid arthritis antibodies recognizing a cyclic citrullinated peptide, *Arthritis Rheum.*, 2000, **43**(1), 155–163.
33 F. Anjum, F. Zakir, D. Verma, M. Aqil, M. Singh, P. Jain, *et al.*, Exploration of Nanoethosomal Transgel of Naproxen Sodium for the Treatment of Arthritis, *Curr. Drug Delivery*, 2020, **17**(10), 885–897.

34 M. Endo, T. Yamamoto and T. Ijuin, Effect of nonionic surfactants on the percutaneous absorption of Tenoxicam, *Chem. Pharm. Bull.*, 1996, **4**(4), 1878–1892.
35 L. Yang, L. Wu, D. Wu, D. Shi, T. Wang and X. Zhu, Mechanism of transdermal permeation promotion of lipophilic drugs by ethosomes, *Int. J. Nanomed.*, 2017, 3357–3364.
36 M. J. Alvarez-Figueroa, D. A. Alarcón and J. V. González-Aramúndiz, Effect of zeta potential of innovative lipid nanocapsules on triamcinolone transdermal delivery, *Drug Delivery Transl. Res.*, 2022, **12**(11), 2740–2750.
37 C. L. Froebe, F. A. Simion, L. D. Rhein, R. H. Cagan and A. Kligman, Stratum corneum lipid removal by surfactants: Relation to in vivo irritation, *Dermatology*, 1990, **181**(4), 277–283.